

Photonic Crystal and Plasmonic Silicon-Based Light Sources

Maria Makarova, *Student Member, IEEE*, Yiyang Gong, Szu-Lin Cheng, Yoshio Nishi, *Fellow, IEEE*, Selçuk Yerci, *Student Member, IEEE*, Rui Li, Luca Dal Negro, *Member, IEEE*, and Jelena Vučković, *Member, IEEE*

Abstract—Efficient silicon (Si)-compatible emitters can realize inexpensive light sources for a variety of applications. In this paper, we study both photonic crystal (PC) and plasmonic nanocavities that enhance the emission of Si-compatible materials. In particular, we examine the coupling of silicon nanocrystals (Si-NCs) to silicon nitride PC cavities and Si-NCs in silicon dioxide to plasmonic gratings, both for enhancement of emission in the visible wavelengths. In addition, we also observe the enhancement of the 1530 nm emission from erbium-doped silicon nitride films coupled to Si PC cavities. Finally, we analyze the loss mechanisms associated with the hybrid silicon nitride/silicon system, and propose advancements in the designs of PC and plasmonic cavities for the emitters described in this paper.

Index Terms—Cavity resonator, erbium, light sources, MIM devices, plasmonics.

I. INTRODUCTION

SILICON (Si)-based light sources compatible with mainstream CMOS technology are highly desirable because of their low manufacturing cost relative to III/V semiconductors and because they will enable monolithic integration with electronic components on the same Si platform. In this paper, we describe optical devices based on materials that can share fabrication tools with Si-CMOS processing without a risk of contamination and have promising optical properties. We studied light-emitting Si-rich Si nitride (SRN), Si nanocrystals (Si-NCs) embedded in silicon dioxide, and erbium-doped amorphous Si nitride (Er:SiN_x) systems. Both Si-NCs in SiO₂ [1]–[6] and silicon nitride [7]–[10] are well studied and show photoluminescence (PL) with wavelengths from 500 to 1000 nm. In these

samples, the emission is enhanced relative to the emission from bulk Si because of electron-hole localization effects due to either quantum confinement or trapping to surface states [11]. In addition, significant work has been conducted to study electrical injection of the Si-NCs in both oxide and nitride systems [12]–[14]. We also explore a material system with Er in amorphous silicon nitride, which emits at the telecom wavelength of 1530 nm, ideally suited for on-chip Si photonics applications [15], [16]. The limitation of Er, as a gain material for on-chip photonics applications, is its small absorption cross section, which limits its pump rate and gain parameters. However, it is possible to enhance the pumping of Er ions in amorphous silicon nitride by taking advantage of an efficient, nanosecond-fast energy transfer from the matrix, which has four orders of magnitude larger absorption cross section than direct excitation of Er ions [15]–[17]. Since SRN layers can be electrically injected more efficiently than oxide-based dielectric matrices [14], it should also be possible to electrically excite Er ions in this configuration, paving a path to electrically pumped sources at the telecom wavelength.

In this paper, we focus on using photonic crystal (PC) cavities and plasmonic gratings to enhance luminescence from such CMOS-compatible materials. Nanocavities modify the local optical density of states (DOS) to enhance the emission in a fundamentally different way than what is accessible through materials engineering. Specifically, photon emission rate can be enhanced at a particular wavelength because the optical DOS is higher at the cavity resonance, which, in turn, improves efficiency and allows faster modulation rates [18]. The emission rate enhancement in a resonator, as predicted by Purcell [19], is given by

$$F = \frac{3}{4\pi^2} \left(\frac{\lambda}{n}\right)^3 \frac{Q}{V_{\text{mode}}} \left(\frac{E}{E_{\text{max}}}\right)^2 \overline{\psi(\theta, \lambda)} \quad (1)$$

where $Q = \omega/\Delta\omega$ is the quality factor of the cavity mode, V_{mode} is the mode volume of the cavity, and $\overline{\psi(\theta, \lambda)}$ includes the average alignment of a dipole emitter with the cavity field (taken in the case of our cavities to be approximately 1/3) and the decrease of enhancement for spectrally detuned emitters that follows a normalized Lorentzian with the cavity lineshape. By increasing the quality factor and reducing the cavity-mode volume, the Q/V figure of merit can be substantially increased in both PC cavities and plasmonic gratings. While previous works have extensively studied Si-NCs coupled to microdisk cavities, such cavities have very large mode volumes when achieving high Q s [20]. PC cavities have significantly smaller mode volumes when maintaining high Q s, and thus can, in principle, achieve higher Purcell enhancements. Similarly, while plasmonic modes

Manuscript received May 7, 2009; revised June 19, 2009 and August 12, 2009. Current version published February 5, 2010. This work was supported in part by Grants from the MARCO Interconnect Focus Center, by the Air Force Office of Scientific Research, by the U.S. Air Force Multidisciplinary University Research Initiative Program “Electrically Pumped Silicon-Based Lasers for Chip-Scale Nanophotonic Systems” supervised by Dr. G. Pomrenke, and by Stanford Nanofabrication Facility of the National Nanotechnology Infrastructure Network supported by the National Science Foundation under Grant ECS-9731293. M. Makarova, and Y. Gong contributed equally to this work.

M. Makarova, Y. Gong, and J. Vučković are with the Department of Electrical Engineering, Stanford University, Stanford, CA 94305 USA (e-mail: makarova@stanford.edu; yiyangg@stanford.edu; jela@stanford.edu).

S.-L. Cheng is with the Department of Material Science and Engineering, Stanford University, Stanford, CA 94305 USA (e-mail: slcheng@stanford.edu).

Y. Nishi is with the Department of Electrical Engineering and the Department of Material Science and Engineering, Stanford University, Stanford, CA 94305 USA (e-mail: nishiy@stanford.edu).

S. Yerci, R. Li, and L. D. Negro are with the Department of Electrical and Computer Engineering, Boston University, Boston, MA 02215 USA (e-mail: syerci@bu.edu; ruli@bu.edu; dalnegro@bu.edu).

Color versions of one or more of the figures in this paper are available online at <http://ieeexplore.ieee.org>.

Digital Object Identifier 10.1109/JSTQE.2009.2030777

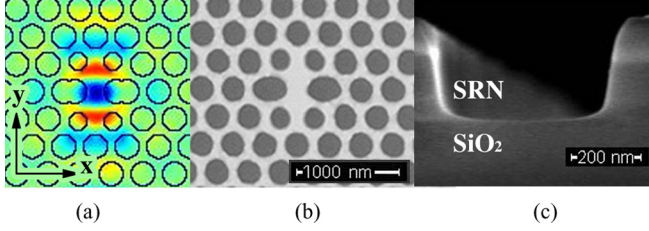


Fig. 1. (a) FDTD calculated profile for the x -component of the electric field that is dominant at the center of the cavity. (b) Fabricated cavity with periodicity of 334 nm. (c) Trench cross section showing non vertical etch profile.

suffer from degradation of Q s due to ohmic metallic losses, this can be compensated for with mode volumes that break the diffraction limit. Previous papers have demonstrated enhancements of Si-NC emission with patterned metallic particle arrays [21]. However, Ref. [21] did not analyze the wavelength selectivity of the plasmonic modes. To further explore the emission of Si-NCs and SiN_x-sensitized Er, we have attempted to couple the emitters to nanocavities, as described in the following sections. Section II describes enhancement of PL from Si-NCs using PC cavities, while Section III describes the analogous effect from plasmonic gratings. Finally, Section IV covers Er PL enhancement in PC cavities.

II. PC CAVITY LIGHT SOURCE IN THE VISIBLE

As described previously, Si-NCs emit at the visible wavelengths and can possibly be employed in inexpensive light sources. For this section, we focus on implementing PC cavity designs to enhance the emission of Si-NCs in Si-rich nitride. Since Si itself has high absorption in the 600–900 nm range, alternative materials that are transparent in the visible wavelengths, such as SRN, must be used to enhance Si-NC light emission. Due to the low index of refraction of the SRN layer ($n = 2.1$), it is more challenging to achieve high Q s in silicon nitride than in Si. We designed and fabricated cavities for this material with modest Q -factors [22], and since then others have achieved Q s as high as 3400 [23]. It is important to point out that for PC design, using SRN is more advantageous than the Si-NCs in SiO₂ matrix because it has a higher refractive index.

Finite-difference time-domain (FDTD) simulations [24] were used to optimize a single-hole defect design [see Fig. 1(a)], as in [25], for a 240-nm-thick SRN membrane with refractive index $n = 2.11$. The computations were performed for the single defect cavity with seven layers of PC mirror holes around it. Discretization of 20 units per period a was used. The nearest neighbor holes on the horizontal axis of the cavity were smeared inward by $H_{\text{shift}} = 0-0.20a$, while the nearest neighbor holes in the diagonal directions were shifted out by $D_{\text{shift}} = 0-0.10a$, and their radius varied from $r/a_D = 0.25-0.30$. The radius of PC lattice holes was varied from $r/a = 0.35-0.40$, and the slab thickness was fixed at $d/a = 0.75$. In this optimization space, the highest Q was found for $H_{\text{shift}} = 0.30a$, $D_{\text{shift}} = 0.05a$, $r/a_D = 0.275$, and $r/a = 0.375$. The optimized structure has a resonance frequency of $a/\lambda = 0.45$, in-plane $Q = 2400$, out-of-plane $Q = 2200$, and mode volume $V_{\text{mode}} = 0.784(\lambda/n)^3$.

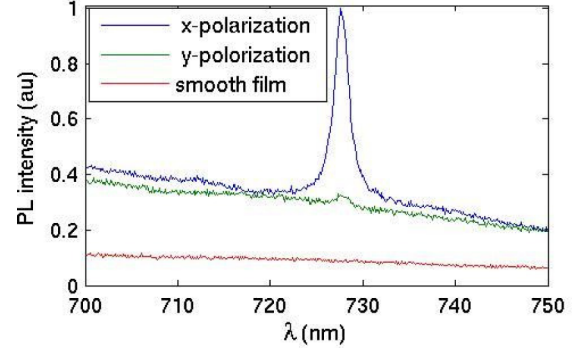


Fig. 2. PL from the cavity, as shown in Fig. 1, in the x - and y -polarizations, and from an unpatterned region of the sample.

The maximum Purcell enhancement for this cavity is 1100 for an emitter spectrally and spatially aligned to the cavity.

The structures were fabricated, starting from bare silicon wafers. First, a 500-nm-thick oxide layer was formed by wet oxidation, and then, a 250-nm-thick layer of SRN was deposited by chemical vapor deposition (CVD) with NH₃ and SiH₂Cl₂ gases at 850 °C. Next, a positive electron beam resist, ZEP-520A, was spun on a wafer piece to form a 380-nm-thick mask layer, and the PC cavity pattern was exposed on the Raith 150 electron beam system. After development, the pattern formed in the resist layer was transferred into the silicon nitride layer by reactive ion etching with NF₃ plasma using ZEP pattern as a mask. Any remaining resist was removed by oxygen plasma. The oxide layer was removed under PC structures by a 6:1 buffered oxide etch [22]. A typical fabricated structure with periodicity $a = 334$ nm is shown in Fig. 1(b). The measured quality factor for the fabricated cavity was 396, as obtained from a Lorentzian fit to the cavity spectrum in Fig. 2. The measured cavity Q is substantially lower than predicted by FDTD due to imperfect PC hole circularity [see Fig. 1(b)] and nonvertical etching profile, as observed in a cross section of a trench etched under the same experimental conditions [see Fig. 1(c)]. Barth *et al.* [26] show that nonvertical etch profile is especially detrimental to cavity Q factors.

A micro-PL (μ -PL) setup was used to measure PL spectra from the fabricated structure. A single 100 \times objective lens with numerical aperture $NA = 0.5$ was used to image the sample, focus the pump beam, and collect luminescence perpendicular to the PC membrane. The signal sent to the spectrometer was spatially filtered by an iris that limits the collection area to the PC cavity. As confirmed by FDTD simulations, the cavity resonance is clearly seen in the x -polarization, while the PL from the unpatterned film and the orthogonal y -polarization do not show any resonances (see Fig 2). The cavity resonance enhances PL intensity by 11-fold relative to smooth film and threefold relative to the orthogonal polarization. This enhancement is roughly two times stronger than what was demonstrated previously in unoptimized L3 PC cavities in the same SRN film [22]. The enhancement may be attributed to improved PL collection efficiency for the cavity mode and increased radiative rate due to Purcell effect.

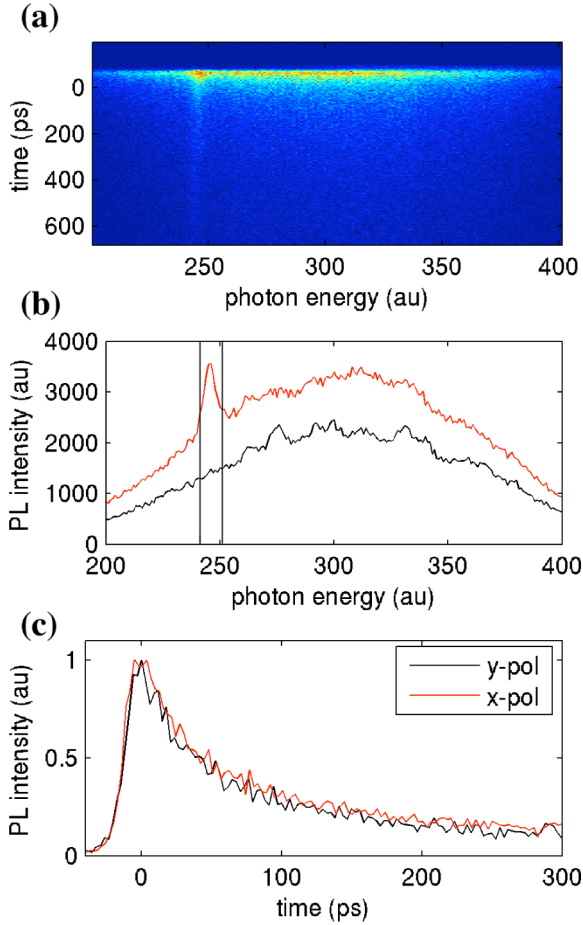


Fig. 3. Time-resolved measurement of PL collected from the cavity. (a) Streak camera data of PL collected from PC cavity. (b) Spectra for x - (red) and y - (black)-polarized PL obtained from the streak camera by summing up signal over time. (c) Time traces of PL for x - (red) and y - (black)-polarization averaged over the spectral region highlighted in (b).

To quantify the Purcell enhancement, we perform time-resolved PL measurements using frequency-doubled picosecond pulses from mode-locked Ti:Sapphire laser for excitation at 400 nm and a streak camera for signal detection. These measurements give the total PL intensity decay rate, which is a combination of the radiative and nonradiative decays

$$\frac{1}{\tau} = \frac{1}{\tau_{nr}} + \frac{1}{\tau_{rad}} \quad (2)$$

where τ , τ_{nr} , and τ_{rad} are the total, nonradiative, and radiative lifetimes, respectively. The time-resolved spectral data, shown in Fig. 3, were measured at the temperature of 10 K to reduce the nonradiative recombination rate. The emission collected from the x -polarized cavity resonance and at the orthogonal polarization over the spectral region, as shown in Fig. 3(b), has the time series shown in Fig. 3(c).

The PL decay time at room temperature was 26.5 ps, and at 10 K, it increased to 88.5 ps. This is 19 times faster than the reported lifetime of about 0.5 ns for similar nitride films with 7% efficiency [7]. We can estimate the radiative lifetime of such SRN film to be $\tau_{rad} = \tau_{measured}/\eta = 7$ ns, where η is the radiative emission efficiency. Assuming the same radiative

lifetime, our films have efficiency of 0.37% at room temperature and 1.2% at 10 K. Therefore, the PL decay measurement is completely dominated by the nonradiative decay, and we cannot observe the enhancement of the radiative lifetime. However, the increase in radiative rate should manifest itself with efficiency increase. We observe a threefold PL signal enhancement at the cavity resonance over the uncoupled emission. It is still possible that some of this enhancement may be due to the Purcell effect, while some enhancement may be due to more efficient collection of the cavity emission relative to the emission from uncoupled nanocrystals. Experimentally, it is difficult to discriminate these two effects in samples that have high nonradiative recombination rate.

From the lifetime measurements, it is clear that the radiative efficiency of the nitride film must be improved to make a more viable light source and to be able to observe the Purcell effect directly. Perhaps, a better approach would be to use Si-NCs with SiO₂ shell, which have microsecond radiative lifetimes, demonstrated material gain, and are quite well understood [2]–[6]. These Si-NCs could be fabricated by anodic etching of Si, deposited onto silicon nitride slab from solution, and capped with another silicon nitride layer deposited by plasma-enhanced CVD (PECVD) at low temperature, as was done for capacitive memory applications [27]. This is attractive because high-quality Si-NCs can be incorporated into the center of the PC cavity, where the cavity field is maximum, and nanocrystals can be filtered by size before deposition to decrease inhomogeneous broadening of PL.

III. PLASMONIC GRATINGS FOR INTERACTION WITH SI-NCs

In addition to PC cavities, plasmonic devices also have the potential to realize inexpensive, efficient light sources. Much like the PC counterparts, the plasmonic devices also enhance the luminescence of emitters by increasing the extraction efficiency and the Purcell enhancement. Surface plasmon polariton (SPP) modes, bound to a flat metal–dielectric interface, are characterized by the following dispersion relation [28]:

$$k_{sp} = \frac{\omega}{c} \sqrt{\frac{\epsilon_d \epsilon_m(\omega)}{\epsilon_d + \epsilon_m(\omega)}} \quad (3)$$

where $\epsilon_d = n^2$ is the dielectric constant of the dielectric layer, and the dielectric constant of the metal is given by the Drude model $\epsilon_m(\omega) = 1 - (\omega_p/\omega)^2$. Gold was used as the metal for this paper, and has plasma frequency $\omega_p = 2\pi c/(160 \times 10^{-9} \text{ m})$. At the high symmetry points of the dispersion relation, we have $k_{sp} = p\pi/a$, where p is an integer number indicating the order of the plasmonic mode and a is the grating periodicity of the p th-order plasmonic mode. The large propagation vector k_{sp} also leads to the field profile exponentially decaying in both the metal and dielectric materials, and thus giving the SPP modes potentially low mode volumes that break the diffraction limit. In recent years, InGaN-based quantum wells (QWs) and CdSe colloidal quantum dots have been coupled to the high density of optical states at the surface plasmon frequency [29]–[31]. In order to extract emission efficiently and diversify the SPP enhancement over a range of wavelengths, various groups have

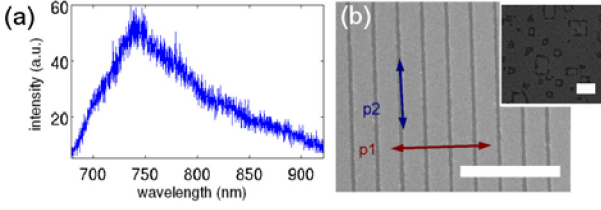


Fig. 4. (a) Bulk PL from Si-NCs in SiO₂. (b) Fabricated gold grating, with the marker representing 1 μm. The measured p1 and p2 polarizations selected in experiment are shown on top of the grating. (Inset) Degradation of the gold substrate with high annealing temperature, with the marker representing 2 μm.

investigated grating-type structures combined with QWs or organic materials [32]–[35]. In addition, since metals are already a part of the device design, it is practical to configure plasmonic devices to be electrically injected [13]. In this paper, we expand on our work done previously with Si-NCs in oxide coupled to metallic gratings [36].

While the previous structures with metallic gratings on only one side of the emitters can have high light in- and out-coupling, the decaying tail of the SPP mode still limits the average electric field obtained in the active material. In order to increase this figure of merit, we propose to use an MIM configuration with a metal substrate and a patterned metal grating on top of the Si-NC layer, as in a previous work with InGaAs QWs [32]. Since the Si-NCs are robust and can form even in a poor quality of oxide, such a structure allows bottom-up fabrication by first depositing the gold substrate, then depositing a Si-rich oxide (SRO) layer, and finally patterning the metallic grating on top. Hence, Si-NCs are ideally suited for incorporation inside of the MIM structures, as the fabrication does not require complicated lift-off procedures, as in the procedures required to incorporate QWs [32].

A 40-nm-thick layer of SRO, with effective index of refraction, $n_{\text{eff}} = 1.7$, is grown on 100 nm of gold on top of a thick SiO₂ layer by plasma enhanced CVD (PECVD) with a 14:1 mixture of SiH₄ (diluted to 2% with N₂) and N₂O at 350 °C. The 100 nm gold layer is sufficiently thick to act as an optical blocking layer. At high annealing temperatures, the gold substrate degrades, leading to breaks in the substrate [see Fig. 4(b), inset]. This particular sample was not annealed at high temperature, and thus maintained high film quality [see Fig. 4(b)]. The PL of the Si-NCs on the gold substrate is shown in Fig. 4(a), and is sufficient to probe the MIM SPP mode from $\lambda_0 = 700$ –1000 nm. Then, a 100-nm layer of polymethylmethacrylate (PMMA) is spun on top of the wafer followed by e-beam lithography to define the grating pattern. Finally, a 30-nm layer of gold (Au) is evaporated on top of the PMMA layer and the grating is fabricated by liftoff in acetone. We pump Si-NCs with a green laser at 532 nm and collect the emission from the top side of the sample with an objective lens with large numerical aperture NA = 0.5, thereby maximizing the collection.

We first analyze the exact structure in 2-D FDTD simulations, as in previous references [32], [37]. Setting the duty cycle (the ratio of the gold bars width to the grating period) to be 0.8, we calculate the band edge frequencies of the modes at the Γ ($k = 0$) and X ($k = \pi/a$) points of the band diagram for grating periods

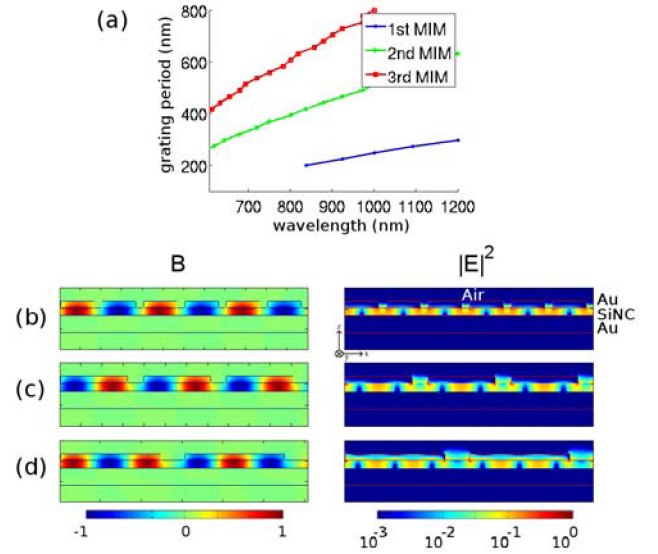


Fig. 5. (a) FDTD calculated band edge frequencies for first-, second-, and third-order modes of the MIM device with a 40-nm-thick Si-NC spacer layer. The first- and third-order modes correspond to modes at the X ($k = \pi/a$) point of the dispersion relation, while the second-order mode corresponds to modes at the Γ ($k = 0$) point. The $|E|^2$ and B fields for the (b) first-, (c) second-, and (d) third-order modes are plotted.

from 200 to 800 nm. We plot the free-space mode wavelengths (λ_0) for the first three SP modes in Fig. 5(a), with the first-order mode fitting one half SPP wavelength per grating period (corresponding to $k = \pi/a$, i.e., the X point of the band diagram), the second-order mode fitting a full SPP wavelength per grating period ($k = 2\pi/a$, which folds to the Γ point), etc. We also calculate the field profiles for the first three-order modes, fixing the free-space wavelength $\lambda_0 \approx 800$ nm, and plotting the results in Fig. 5(b)–(d). We first note the redshift of the mode wavelength as the period of the grating is increased. Furthermore, the mode profiles of all the examined modes correspond to an even symmetry through the center of the Si-NC layer. We also observe that the mode wavelengths of the MIM devices are redshifted from the values calculated for the single-sided grating designs of the same grating period. Such a shift can be explained as the coupling between the SPP modes on the two metal–dielectric interfaces, leading to a “bonding” symmetric plasmonic mode with higher effective index than the effective index of the individual SPP modes.

Next, we calculate the Purcell enhancement. We make the intuitive approximation that the standing wave modes in Fig. 5(b)–(d) are modes of cavities spaced with the period of the SPP half wavelength, as these modes have the same λ_0 . We then calculate radiative quality factor (Q_{rad}) and the mode volume, which is defined as

$$V_{\text{quant}} = \frac{\iint \epsilon_E(x, z) |E(x, z)|^2 dx dz}{\max [\epsilon_E(x, z) |E(x, z)|^2]} Y = A \times Y \quad (4)$$

where the integral is taken over the half wavelength of the SPP wave, $\epsilon_E(x, z) = d(\omega\epsilon(x, z))/d\omega$ is the effective dielectric constant, Y is the length of the grating bars, and A is the effective mode area. Using the earlier figures, and noting that the

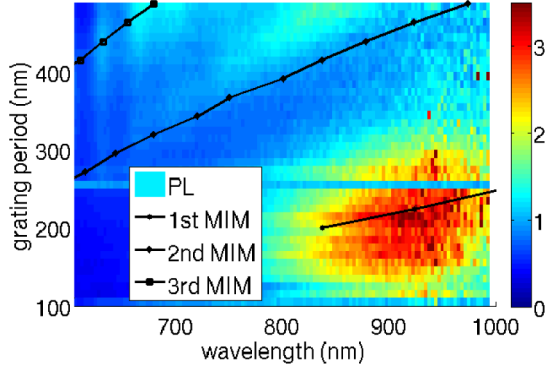


Fig. 6. Collected PL from MIM grating devices with different periodicity normalized to the bulk PL. The corresponding FDTD band calculations from Fig. 5(a) are replotted.

quality factor is limited to the absorption factor $Q_{\text{abs}} \approx 50$ (since $Q_{\text{rad}} \approx 500 \gg Q_{\text{abs}}$), we can calculate the average Purcell enhancement by using (1), where the E -field intensity is again averaged over the region occupied by the Si-NCs. In this case, the Purcell enhancement is defined as the increase of emission into the cavity mode in addition to the bulk emission. For these modes, we observe that the average coupling between the Si-NC emitters and the MIM SPP mode is increased by a factor of 1.6 relative to the structure with only the grating on top. In addition, the confinement factor Γ , or the fraction of the mode overlapping with the active material, is improved from 0.2 for the one-sided design to 0.5 for the MIM design for all three modes. Finally, due to confinement of the SPP mode from both the top and the bottom, the mode area of the MIM structures is reduced by one-half from the mode area of the one-sided designs. With $Y = 10 \mu\text{m}$ as in the fabricated devices, we estimate the average Purcell enhancement of emitters in the Si-NC film to be 2.2, 2.4, and 2.4 for the first-, second-, and third-order modes, respectively. This is a threefold improvement from the enhancements using a one-sided grating design, which have Purcell enhancements of 0.7, 0.7, and 0.7, for the same grating design and active material thickness.

The SPP grating modes in Fig. 5(b)–(d) are predominantly polarized in the direction perpendicular to the grating bars (E_x), or p1 in Fig. 4(b). In order to separate the enhancement due to SPP modes from other effects, we isolate two polarizations (p1 and p2) in experiment by collecting with different polarizer settings, as in Fig. 4(b). In our previous experiments with samples of SRO on top of quartz, we collected through the quartz substrate, and thus collected both p1 and p2 [36]. However, for the MIM case, we collect emission from the top side, and only p1 is outcoupled from the grating to the detector. We measure the spectrum for different grating periods, with the emission from the p1 polarization only, as shown in Fig. 6. Using the band edge values from simulation as a guide, enhanced emission is collected from the first- and second-order modes. According to the FDTD-calculated dispersion relationship, the first-order mode lies under the light line and should not be collected. However, the enhanced emission of the first-order mode suggests that surface roughness and local plasmonic modes play roles in scattering emission into the collection optics. The difference in

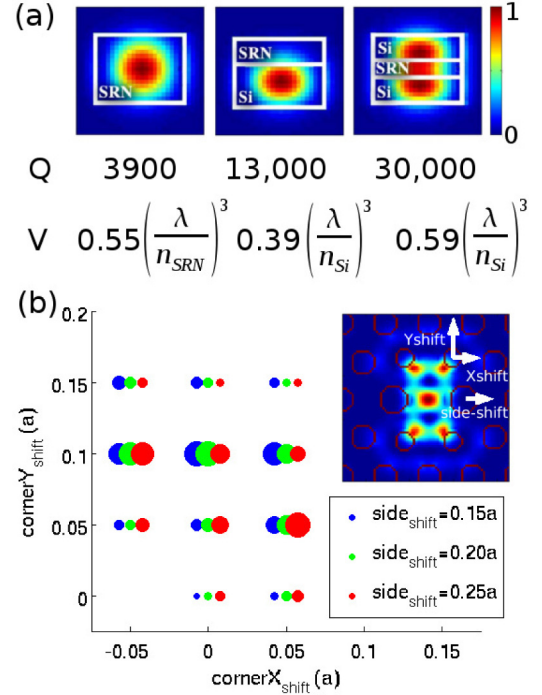


Fig. 7. (a) Design of PC cavities for interaction with Er, with the entire membrane composed of (left), hybrid membrane with silicon nitride on top of Si (middle), and hybrid membrane with silicon nitride in between two Si layers (right). Optimized Q and V are shown. (b) Q -factor optimization for the S1 cavity in the hybrid membrane design [Fig. 7(a), middle] by parameters space search. The cavity mode profile ($|E|^2$) is shown in the inset, along with the directions of the shifts considered. The highest Q -factor is for the design with $x_{\text{shift}} = 0$, $y_{\text{shift}} = 0.1a$, and $\text{side}_{\text{shift}} = 0.15a$, with $Q = 13000$.

the emission peak and the simulation values can be attributed to several factors. A penetration of gold from the substrate into the Si-NC layer could cause an index change in the Si-NC spacer layer, or change the effective thickness of the spacer layer. Since the enhancement of the collected emission relative to bulk is low, designs that improve the PL emitted to the Γ -point of the dispersion relation, such as biharmonic gratings [36], [39], must be investigated.

IV. PC CAVITY LIGHT SOURCE AT TELECOM WAVELENGTH

For operation at the telecom wavelengths (around $1.5 \mu\text{m}$), we are investigating materials consisting of Er ions in light-emitting Si-rich amorphous Si nitride films (Er:SiN_x). Depending on fabrication conditions, the microstructure of this novel materials platform can be engineered to yield either small (2 nm) Si light-emitting nanoclusters or amorphous, homogeneous, light-emitting films ideally suited for the optical activation of Er ions. We have recently demonstrated enhancement of Er emission in SRN PC cavities [40]. Here, we focus on a sample with Er in amorphous SiN_x , which has enhanced emission and reduced nonradiative decay relative to the sample used in [40].

The longer operation wavelength enables us to consider the use of Si as part of the PC membrane, which is attractive because of its higher refractive index. We have investigated three options for the membrane design depicted in Fig. 7(a) [40]. The first option is to have the active Er-doped material to comprise the

entire membrane [see Fig. 7(a), left]. This design has the largest interaction volume of the cavity mode with the active material, but it was difficult to fabricate due to the increased resistance to dry etching of Er:SiN_x, as compared to an undoped SiN_x film. The second option is to use a two-layer membrane composed of a bottom Si layer and a top SiN_x layer [see Fig. 7(a), middle]. While the cavity mode overlap with the active material, $\Gamma = 0.04$, is very low, it is far easier to fabricate high- Q PC cavities in this two-layer membrane due to increased refractive index. The third option is to place the active material in the center of Si membrane, which improves overlap with active region [see Fig. 7(a), right]. The third option may also be attractive for electrical injection of carriers into the active region, but the optical pump at $\lambda = 400$ nm, which is well absorbed by SiN_x-sensitizing Er, is also strongly absorbed by Si. Thus, to maintain simple fabrication procedures and test the efficacy of the sensitization of Er, we focus our initial experiments on the two-layer membrane approach.

The design of the cavity is optimized with FDTD simulations, setting the period of the PC to be $a = 420$ nm, the total slab thickness to be $0.85a$, the Er:SiN_x layer thickness to be one-third of the total slab thickness, and the hole radius to be $r/a = 0.3$. The S1 design is chosen for the PC cavity due to the very small mode volume and good Q -factor [22], [41]. In this case, the two holes on the left and right of the cavity defect have $r/a = 0.35a$, and are shifted by the parameter $side_{\text{shift}}$, while the other four nearest neighbors are shifted outward with the parameters x_{shift} and y_{shift} . By optimizing over the parameter space shown in Fig. 7(b), the optimal $Q = 13\,000$ is found with $x_{\text{shift}} = 0$, $y_{\text{shift}} = 0.1a$, and $side_{\text{shift}} = 0.15a$. Such a cavity mode has normalized frequency $a/\lambda = 0.28$ and mode volume $V_m = 0.38(\lambda/n)^3$, with index of refraction of Si as the reference index $n = 3.5$. The electric field magnitude ($|\vec{E}|^2$) is shown in Fig. 7(b) (inset).

The multilayered wafer is fabricated by growing Er:SiN_x on top of a silicon-on-insulator (SOI) wafer by N₂ reactive magnetron cosputtering from Si and Er targets in a Denton Discovery 18 confocal-target sputtering system. The growth is followed by a post-annealing processes in a rapid thermal annealing furnace at 1170 °C for 340 s under forming gas (5% H₂, 95% N₂) atmosphere. The fabrication of the PC device employs electron beam lithography with 350 nm of ZEP-520A as the resist. The written pattern is then dry etched into the SiN_x and Si slab with a HBr:Cl₂ chemistry. The final membrane is formed by undercutting the 2 μm oxide layer with a 6:1 buffered oxide etch.

The optical experiments are conducted by pumping the cavity structure at normal incidence with a diode laser through a 100× objective with NA = 0.5 and collecting emission through the same objective. The PL collected from the cavity structure and smooth film are shown in Fig. 8. The resonance Q -factors can be up to 5000, as determined from a fit to a Lorentzian (see Fig. 8, inset). The PL is enhanced by about 30 times relative to smooth film (bulk) at the cavity resonance. Light-in-light-out characteristics of the cavity are studied at different pump powers for excitation wavelengths at $\lambda = 400$ nm and $\lambda = 980$ nm (see Fig. 9). The power dependence of the cavity PL amplitude is

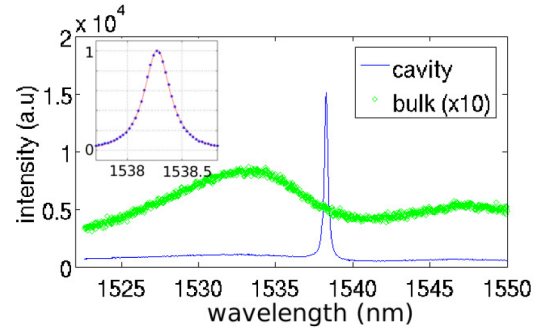


Fig. 8. Cavity and bulk PL from the membrane design shown in Fig. 7(a) (middle). (Inset) Cavity with $Q = 5000$ in a Lorentzian fit.

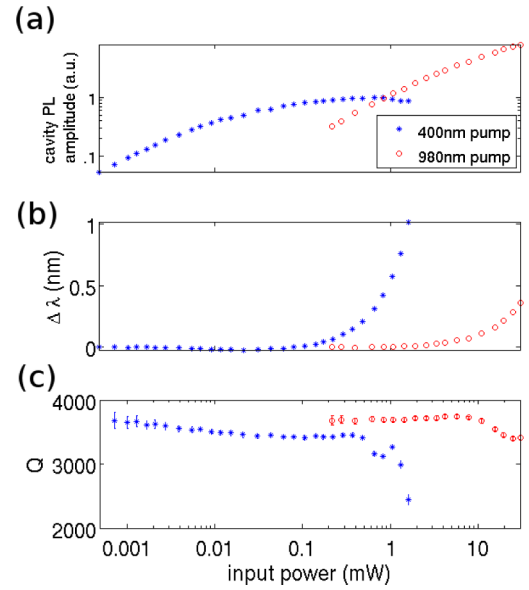


Fig. 9. (a) Cavity PL amplitude power dependence of the same cavity with different pump wavelengths, normalized to the maximum cavity amplitude obtained with the $\lambda = 400$ nm pump. (b) Change in cavity PL wavelength with pump power. (c) Q -factor from fits to a Lorentzian lineshape as a function of input power for $\lambda_{\text{pump}} = 400$ and 980 nm.

shown in Fig. 9(a) for the same cavity with two different pump wavelengths, and the curves are normalized to the maximum power obtained with the $\lambda = 400$ nm pump. In the case of 400 nm excitation, the PL from the cavity saturates at 0.8 mW of pump power. In contrast, with 980 nm excitation, saturation of the cavity resonance can be extended beyond 30 mW (the maximum pump power available from our laser). The maximum output we can achieve from a cavity is about eight times larger with the 980-nm pump laser.

We also observe a blueshift of the cavity wavelength with pump power for low pump powers with the 400 nm pump. Such a shift is associated with the index shift of silicon with the injection of free carriers. While the absorption of free carriers is negligible at these pump powers, the cavity wavelength does decrease by 0.02 nm. At high pump powers for both pump wavelengths, the cavity wavelength increases with pump power, as seen in Fig. 9(b). The redshift of wavelength is indicative of the structure heating up with increasing pump power because

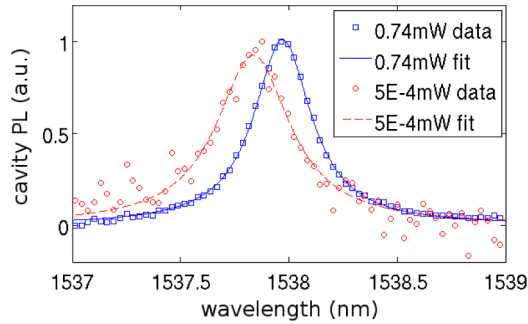


Fig. 10. Spectra of a single cavity pumped with 400 nm laser at 0.74 mW and 5×10^{-4} mW powers, each normalized to the maximum of the corresponding spectrum, along with fits to Lorentzian lineshapes. The fit to the 0.74 mW pump power spectrum has $Q = 4740 \pm 100$, while the fit to the 5×10^{-4} mW pump spectrum has $Q = 3710 \pm 600$.

the refractive index increases with temperature. As expected, the cavity wavelengths start to shift at lower pump powers for the 400-nm pump laser, because Si has a much higher absorption coefficient for $\lambda = 400$ nm than for $\lambda = 980$ nm. The strong absorption of the 400 nm pump is also evident in the cavity Q dependence with pump power, as seen in Fig. 9(c). For the case of the 400 nm pump, the Q starts to drop significantly at about the pump power that saturates the cavity output, suggesting that the cavity output is limited by free-carrier absorption in the Si part of the PC membrane. For the case with the 980 nm pump, we only observe the degradation of Q -factor for pump powers above 10 mW, as the reduced absorption of Si at 980 nm reduces the free-carrier absorption.

Despite the free-carrier absorption induced by the pump at the cavity wavelength, we observe differential gain in some structures with pump power. Fig. 10 shows two spectra with 400 nm excitation, from a different cavity than the cavity measured in Fig. 9. One spectrum is at high pump power (0.74 mW) and one is at low pump power (5×10^{-4} mW), with both normalized to their individual maxima. In addition to the redshift in the cavity peak wavelength due to heating, Lorentzian fits to the data show that the Q increases from 3710 at low pump power to 4740 at high pump power for this cavity. We believe that the observed linewidth narrowing is due to bleaching of Er absorption by the pump, as discussed in detail in [42]. Here, we measure an increase in Q between the two pump powers of $\Delta Q = 1000$. However, as we note from the comparable cavity in Fig. 9, the free-carrier absorption has begun to notably decrease Q at 400 nm excitation wavelength and 0.74 mW pump power. Thus, we would expect an even higher increase in Q in the absence of free-carrier absorption effects.

To conclude, we note that in our current PC design, we are limited by free-carrier absorption in how much light can be extracted from the cavity, especially at 400 nm excitation. Therefore, it would be best to eliminate the Si-layer of the membrane, or use 980 nm excitation to minimize losses due to free-carrier absorption, as we strive to show useful gain in this material.

V. DISCUSSION

We have demonstrated a variety of Si-compatible light sources. Due to the low index of refraction for silicon nanopar-

ticle host materials, fabricating PC devices directly in many oxide and nitride materials is challenging. Nevertheless, Purcell enhancements are expected for both the photonic crystal and plasmonic devices coupled to silicon nanoparticle emitters. In fact, as seen by the increase in the lifetime of Si-NCs over the past years, the quality and internal quantum efficiency of this material is steadily improving. By taking advantage of the Purcell enhancement, it is possible to produce efficient light-emitting devices.

Similarly, with Er:SiN_x, it is possible to provide a Si-compatible platform for on-chip communications. Nevertheless, several challenges remain. Due to the local crystal potentials, the homogeneous broadening of Er ions in SiN_x is approximately 2–10 nm. Thus, the Purcell enhancement for Er is generally low, as the high quality factor of the PC cavity mode must be replaced by the effective quality factor of the emitter in this “bad emitter” regime [43]. This aspect of the emitter makes reaching the lasing threshold much more difficult for the devices in our studies. However, plasmonics may prove to be a solution for this material system as plasmonic resonances are generally broad due to metallic absorption losses. By creating the same plasmonic devices around Er:SiN_x, it may be possible to achieve high Purcell enhancements by virtue of the SP modes’ low mode volumes. Furthermore, plasmonic modes at 1550 nm have the dual benefits of having lower absorption losses than at visible wavelengths and low mode volumes despite material systems with low indexes of refraction. Finally, we would like to move toward a symmetric structure with the nitride layer in the middle of the silicon membrane, improving the overlap of the emitters with the electric field of the PC cavity mode. However, such a design would require a silicon capping layer on top of the active layer. Due to the limitations of available fabrication techniques, such as depositing a noncrystalline Si layer or wafer bonding a crystalline Si layer, the capping layer of silicon would certainly introduce increased absorption losses for the cavity.

Finally, while the MIM system with SRO has the potential to be a device with simple bottom-up fabrication procedures, the silicon oxide materials have certain fabrication restrictions and challenges. One problem with this system is that the SRO layer is much less resistive to gold diffusion than crystalline oxide. While the gold particles penetrating the SRO layer enhances the PL of the Si-NCs, the MIM enhancement is reduced due the lack of coupled SP modes. Thus, the final annealing temperature must be kept low, which also decreases the efficiency of the Si-NCs. In addition, while the predicted Purcell enhancement is high, the metallic structures above and below the emitters greatly reduce the outcoupled PL. In future, a compromise between the confinement and extraction efficiency must be optimized, or an optimized design with high extraction efficiencies must be investigated.

In conclusion, despite challenges with the Si-compatible material systems, we have demonstrated control and enhancement of emission for both visible and telecom wavelengths. The earlier results certainly provide a stepping stone toward more efficient emitters, as well as lasers that operate over a variety of wavelengths. By improving the coupling between these Si-compatible emitters and nanocavities, as well as reducing the

losses of the cavities, we expect to realize useful devices in the near future in systems of nanocavities and these materials for lighting and communication applications.

ACKNOWLEDGMENT

The authors would like to acknowledge V. Sih for developing the fabrication procedures for the Er in nitride samples, H. Sanda for the deposition of silicon-rich nitride film with visible photoluminescence, and T. Carver for metal evaporations. They also would like to acknowledge support from the Intel (MM) and the National Defense Science and Engineering Graduate (YG) Fellowships.

REFERENCES

- [1] M. L. Brongersma, A. Polman, K. S. Min, and H. A. Atwater, "Depth distribution of luminescent Si nanocrystals in Si implanted SiO₂ films on Si," *J. Appl. Phys.*, vol. 86, pp. 759–763, 1999.
- [2] L. Pavesi, L. Dal Negro, C. Mazzoleni, G. Franzò, and F. Priolo, "Optical gain in silicon nanocrystals," *Nature*, vol. 408, pp. 440–444, 2000.
- [3] J. Valenta, R. Juhasz, and J. Linnros, "Photoluminescence spectroscopy of single silicon quantum dots," *Appl. Phys. Lett.*, vol. 80, pp. 1070–1072, 2002.
- [4] R. J. Walters, J. Kalkman, A. Polman, H. A. Atwater, and M. J. A. de Dood, "Photoluminescence quantum efficiency of dense silicon nanocrystal ensembles in SiO₂," *Phys. Rev. B, Condens. Matter*, vol. 73, pp. 132302–1–132302–4, 2006.
- [5] A. G. Cullis, L. T. Canham, and P. D. J. Calcott, "The structural and luminescence properties of porous silicon," *J. Appl. Phys.*, vol. 82, no. 3, pp. 909–965, 1997.
- [6] P. Bettotti, M. Cazzanelli, L. Dal Negro, B. Danese, Z. Gaburro, C. J. Oton, G. Vijaya Prakash, and L. Pavesi, "Silicon nanostructures for photonics," *J. Phys.: Condens. Matter*, vol. 14, pp. 8253–8281, 2002.
- [7] L. Dal Negro, J. H. Yi, J. Michel, L. C. Kimerling, T.-W. F. Chang, V. Sukhovatkin, and E. H. Sargent, "Light emission efficiency and dynamics in silicon-rich silicon nitride films," *Appl. Phys. Lett.*, vol. 88, pp. 233109–1–233109–3, 2006.
- [8] L. Dal Negro, J. H. Yi, L. C. Kimerling, S. Hamel, A. Williamson, and G. Galli, "Light emission from silicon-rich nitride nanostructures," *Appl. Phys. Lett.*, vol. 88, pp. 183103–1–183103–3, 2006.
- [9] N. M. Park, C. J. Choi, T. Y. Seong, and S. J. Park, "Quantum confinement in amorphous silicon quantum dots embedded in silicon nitride," *Phys. Rev. Lett.*, vol. 86, pp. 1355–1355, 2001.
- [10] L. Dal Negro, J. H. Yi, J. Michel, L. C. Kimerling, S. Hamel, A. Williamson, and G. Galli, "Light-emitting silicon nanocrystals and photonic structures in silicon nitride," *IEEE J. Sel. Topics Quantum Electron.*, vol. 12, no. 6, pp. 1628–1635, Nov./Dec. 2006.
- [11] M. V. Wolkin, J. Jorne, P. M. Fauchet, G. Allan, and C. Delerue, "Electronic states and luminescence in porous silicon quantum dots: The role of oxygen," *Phys. Rev. Lett.*, vol. 82, pp. 197–200, 1999.
- [12] K. S. Cho, N. M. Park, T. Y. Kim, K. H. Kim, G. Y. Sung, and J. H. Shin, "High efficiency visible electroluminescence from silicon nanocrystals embedded in silicon nitride using a transparent doping layer," *Appl. Phys. Lett.*, vol. 86, pp. 071909–1–071909–3, 2005.
- [13] R. J. Walters, G. I. Bourianoff, and H. A. Atwater, "Field-effect electroluminescence in silicon nanocrystals," *Nat. Mater.*, vol. 4, pp. 143–146, 2005.
- [14] J. Warga, R. Li, S. N. Basu, and L. Dal Negro, "Electroluminescence from silicon-rich nitride/silicon superlattice structures," *Appl. Phys. Lett.*, vol. 93, pp. 151116–1–151116–3, 2008.
- [15] S. Yerci, R. Li, S. O. Kucheyev, T. van Buuren, S. N. Basu, and L. Dal Negro, "Energy transfer and 1.54 μm emission in amorphous silicon nitride films," *Appl. Phys. Lett.*, vol. 95, pp. 031107–1–031107–3, 2009.
- [16] R. Li, S. Yerci, and L. Dal Negro, "Temperature dependence of the energy transfer from amorphous silicon nitride to Er ions," *Appl. Phys. Lett.*, vol. 95, pp. 041111–1–041111–3, 2009.
- [17] W. C. Ding, D. Hu, J. Zheng, P. Chen, B. W. Cheng, J. Z. Yu, and Q. M. Wang, "Strong visible and infrared photoluminescence from Er-implanted silicon nitride films," *J. Phys. D, Appl. Phys.*, vol. 41, pp. 135101–1–135101–4, 2008.
- [18] H. Altug, D. Englund, and J. Vučković, "Ultra-fast photonic crystal nanolasers," *Nat. Phys.*, vol. 2, pp. 484–488, 2006.
- [19] E. M. Purcell, "Spontaneous emission probabilities at radio frequencies," *Phys. Rev.*, vol. 69, p. 681, 1946.
- [20] R. D. Kekatpure and M. L. Brongersma, "Fundamental photophysics and optical loss processes in Si-nanocrystal-doped microdisk resonators," *Phys. Rev. A, Gen. Phys.*, vol. 78, pp. 023829–1–023829–13, 2008.
- [21] J. S. Biteen, N. S. Lewis, H. A. Atwater, H. Mertens, and A. Polman, "Spectral tuning of plasmon-enhanced silicon quantum dot luminescence," *Appl. Phys. Lett.*, vol. 88, pp. 131109–1–131109–3, 2006.
- [22] M. Makarova, J. Vuckovic, H. Sanda, and Y. Nishi, "Silicon-based photonic crystal nanocavity light emitters," *Appl. Phys. Lett.*, vol. 89, pp. 221101–1–221101–3, 2006.
- [23] M. Barth, N. Nüsse, J. Stingl, B. Löchel, and O. Benson, "Emission properties of high-Q silicon nitride photonic crystal heterostructure cavities," *Appl. Phys. Lett.*, vol. 93, pp. 021112–1–021112–3, 2008.
- [24] J. Vuckovic, M. Loncar, H. Mabuchi, and A. Scherer, "Design of photonic crystal microcavities for cavity QED," *Phys. Rev. E, Stat. Phys. Plasmas Fluids Relat. Interdiscip. Top.*, vol. 65, pp. 016608–1–016608–12, 2002.
- [25] D. Englund and J. Vuckovic, "A direct analysis of photonic nanostructures," *Opt. Exp.*, vol. 14, pp. 3476–3483, 2006.
- [26] M. Barth, J. Kouba, J. Stingl, B. Löchel, and O. Benson, "Modification of visible spontaneous emission with silicon nitride photonic crystal nanocavities," *Opt. Exp.*, vol. 15, pp. 17231–17240, 2007.
- [27] O. M. Nayfeh, D. A. Antoniadis, K. Mantey, and M. H. Nayfeh, "Memory effects in metal-oxide semiconductor capacitors incorporating dispensed highly monodisperse 1 nm silicon nanoparticles," *Appl. Phys. Lett.*, vol. 90, pp. 153105–1–153105–3, 2007.
- [28] H. Raether, *Surface Plasmons*. Berlin, Germany: Springer-Verlag, 1988.
- [29] I. Gontijo, M. Boroditsky, E. Yablonovitch, S. Keller, U. K. Mishra, and S. P. DenBaars, "Coupling of InGaN quantum-well photoluminescence to silver surface plasmons," *Phys. Rev. B, Condens. Matter*, vol. 60, no. 16, pp. 11564–11567, 1999.
- [30] K. Okamoto, I. Niki, A. Shvartser, Y. Narukawa, T. Mukai, and A. Scherer, "Surface plasmon enhanced light-emitters based on InGaN quantum wells," *Nat. Mater.*, vol. 3, pp. 601–605, 2004.
- [31] K. Okamoto, S. Vyawahare, and A. Scherer, "Surface plasmon enhanced bright emission from CdSe quantum dots nanocrystal," *J. Opt. Soc. Amer. B, Opt. Phys.*, vol. 23, pp. 1674–1678, 2006.
- [32] J. Vučković, M. Lončar, and A. Scherer, "Surface plasmon enhanced light-emitting diode," *IEEE J. Quantum Electron.*, vol. 36, no. 10, pp. 1131–1144, Oct. 2000.
- [33] K.-C. Shen, C.-Y. Chen, C.-F. Huang, J.-Y. Wang, Y.-C. Lu, Y.-W. Kiang, C. C. Yanga, and Y.-J. Yang, "Polarization dependent coupling of surface plasmon on a one-dimensional Ag grating with an InGaN/GaN dual-quantum-well structure," *Appl. Phys. Lett.*, vol. 92, pp. 013108–1–013108–3, 2008.
- [34] Y.-J. Hung, I. I. Smolyaninov, C. C. Davis, and H.-C. Wu, "Fluorescence enhancement by surface gratings," *Opt. Exp.*, vol. 14, pp. 10825–10830, 2006.
- [35] N.-F. Chiu, C.-W. Lin, J.-H. Lee, C.-H. Kuan, K.-C. Wu, and C.-K. Lee, "Enhanced luminescence of organic/metal nanostructure for grating coupler active long-range surface plasmonic device," *Appl. Phys. Lett.*, vol. 91, pp. 083114–1–083114–3, 2007.
- [36] Y. Gong, J. Lu, S.-L. Cheng, Y. Nishi, and J. Vučković, "Plasmonic enhancement of emission from Si-nanocrystals," *Appl. Phys. Lett.*, vol. 94, pp. 013106–1–013106–3, 2009.
- [37] Y. Gong and J. Vučković, "Design of plasmon cavities for solid-state cavity quantum electrodynamics applications," *Appl. Phys. Lett.*, vol. 90, pp. 033113–1–033113–3, 2007.
- [38] H. Iwase, D. Englund, and J. Vučković, "Analysis of Purcell effect for absorptive plasmonic crystals," to be published. Purcell factor and β factor in a photonic crystal waveguide," *Phys. Rev. B, Condens. Matter*, vol. 75, p. 205437, 2007.
- [39] A. Kocabas, S. S. Senlik, and A. Aydinli, "Plasmonic band gap cavities on biharmonic gratings," *Phys. Rev. B, Condens. Matter*, vol. 77, pp. 195130–1–195130–7, 2008.
- [40] M. Makarova, V. Sih, J. Warga, R. Li, L. Dal Negro, and J. Vučković, "Enhanced light emission in photonic crystal nanocavities with Erbium-doped silicon nanocrystals," *Appl. Phys. Lett.*, vol. 92, pp. 161107–1–161107–3, 2008.
- [41] I. Fushman, D. Englund, and J. Vuckovic, "Coupling of Pb quantum dots to photonic crystal cavities at room temperature," *Appl. Phys. Lett.*, vol. 87, pp. 241102–1–241102–3, 2005.
- [42] Y. Gong, M. Makarova, S. Yerci, R. Li, M. J. Stevens, B. Baek, S. W. Nam, R. H. Hadfield, S. N. Dorenbos, V. Zwiller, J. Vučković, and L.

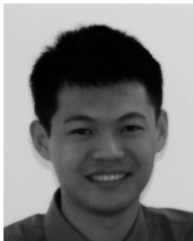
Dal Negro, "Linewidth narrowing and Purcell enhancement in photonic crystal cavities on an Er-doped silicon nitride platform," *Opt. Exp.*, 2010, to be published.

- [43] M. P. van Exter, G. Nienhuis, and J. P. Woerdman, "Two simple expressions for the spontaneous emission factor β ," *Phys. Rev. A, Gen. Phys.*, vol. 54, pp. 3553–3558, 1996.



Maria Makarova (S'07) was born in Novosibirsk, Russia, in 1981. She received the B.S. degree in electrical and computer engineering from the University of Illinois at Urbana-Champaign, Urbana, in 2003, and the M.S. degree in electrical engineering in 2005 from Stanford University, Stanford, CA, where she is currently working toward the Ph.D. degree with the Nanoscale and Quantum Photonics Research Group, Department of Electrical Engineering.

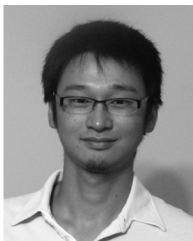
Her research interests include silicon-based photonic crystal light sources, including design, fabrication, and optical characterization.



Yiyang Gong received the B.S. degree in electrical engineering from California Institute of Technology, Pasadena, in 2005, and the M.S. degree in electric engineering from Stanford University, Stanford, CA, in 2008, where he is currently working toward the Ph.D. degree with the Nanoscale and Quantum Photonics Group, Department of Electrical Engineering.

His research interests include photonic crystal and plasmonic devices for optical interconnects, solid-state lighting, and development of high-speed computational tools for designing and simulating optical

systems.



Szu-Lin Cheng received the B.S. and M.S. degrees in material science and engineering from the National Tsing-Hua University, Hsinchu, Taiwan, in 2002 and 2004, respectively. He is currently working toward the Ph.D. degree with the Department of Material Science and Engineering, Stanford University, Stanford, CA.

His current research interest include silicon-compatible optoelectronic devices, ranging from material optics to device physics and characterization, and the CMOS-compatible germanium-based laser

with the applications of telecommunication and optical interconnect systems. Recently, he successfully demonstrated the germanium LED on silicon substrate, which is an important step toward CMOS-compatible lasers.



Yoshio Nishi (F'88) received the B.S. degree in material science from Waseda University, Tokyo, Japan, and the Ph.D. degree in electronics engineering from the University of Tokyo, Tokyo.

He was with Toshiba R&D, where he was involved in semiconductor device physics. During 1986, he was with Hewlett-Packard, where he was the Director of Silicon Process Laboratory, and with Texas Instruments as the Senior Vice President and the Director of R&D for semiconductor group. He is currently a Professor in the Department of Electrical Engineering

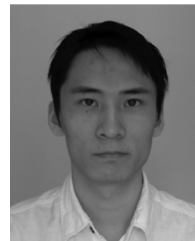
and also in the Department of Material Science and Engineering, Stanford University, Stanford, CA. He is also the Director of Stanford Nanofabrication Facility of the National Nanotechnology Infrastructure Network of U.S. and the Director of Research for the Center for Integrated Systems. His research interest include nanoelectronic devices and materials including metal gate/high-k MOS, device layer transfer, nanowire devices, and resistance change nonvolatile memory materials and devices. He has authored or coauthored more than 200 papers, and coauthored/edited 12 books. He holds more than 70 patents in U.S. and Japan. He has served as a Board member for SRC and International Sematech, as well as on the NNI Panel and MARCO Governing Council.

Dr. Nishi is a Member of Japan Society of Applied Physics and the Electrochemical Society. He was the recipient of numerous honors and awards in U.S. and Japan, including the 1995 IEEE Jack Morton Award, the 2002 IEEE Robert Noyce Medal, the 2005 International Meeting for Future of Electron Devices, Kansai, Best Paper Award, and the 2007 Portland International Center for Management of Engineering and Technology Leadership in Technology Management Award. Currently, he is an affiliated member of the Science Council of Japan.



Selçuk Yerci (S'08) received the B.S. and M.S. degrees in physics from the Middle East Technical University, Ankara, Turkey, in 2004 and 2007, respectively. He is currently working toward the Ph.D. degree in electrical engineering with Boston University, Boston, MA.

His current research interests include fabrication and structural and electrical characterization of optoelectronic materials, and monolithic microphotonic light-emitting devices based on silicon nitride.



Rui Li received the B.S. degree in photonic science and technology from Sun Yat-sen University, Guangzhou, China, in 2005. He is currently working toward the Ph.D. degree in electrical engineering with Boston University, Boston, MA.

His current research interests include linear and nonlinear optical properties of amorphous silicon nitride, Er sensitization in amorphous silicon nitride, simulation and fabrication of waveguide, and resonant photonic structures.



Luca Dal Negro (M'09) received the Laurea degree (*summa cum laude*) in physics, and the Ph.D. degree in semiconductor physics from the University of Trento, Trento, Italy, in 1999 and 2003, respectively.

In 2003, he joined Massachusetts Institute of Technology as a Postdoctoral Associate. Since January 2006, he has been an Assistant Professor with the Department of Electrical and Computer Engineering, Boston University, Boston, MA, where he is a member of the Photonics Center. His current research inter-

est include research projects on silicon-based materials, devices and photonic structures, optical spectroscopy of nanostructures, complex photonic media, and nanoplasmonics. He has authored and coauthored more than 70 technical articles.



Jelena Vučković (S'92–M'03) received the Doctorate degree from California Institute of Technology, Pasadena, CA, in 2002.

Since 2003, she has been with the Department of Electrical Engineering and Ginzton Laboratory, Stanford University, Stanford, CA, where she is currently an Associate Professor and Chambers Faculty Scholar, leading the Nanoscale and Quantum Photonics Research Group. Her research interest include experimental nanophotonics and quantum photonics, including photonic crystals and solid-state photonic

quantum information systems. She has authored or coauthored more than 80 journal publications, seven book chapters, six issued, and various pending U.S. patents, and gave more than 100 invited talks.

Dr. Vučković was the recipient of various awards, including the Presidential Early Career Award for Scientists and Engineers—the highest honor for young scientists and engineers in the U.S., the Office of Naval Research Young Investigator Award, and the Defense Advanced Research Projects Agency Young Faculty Award.